atmosphere

Article

Using HawkEye Level-2 Satellite Data for Remote Sensing Tasks in the Presence of Dust Aerosol

Anna Papkova *, Darya Kalinskaya and Evgeny Shybanov

Marine Hydrophysical Institute of the Russian Academy of Sciences, 2 Kapitanskaya St., 299011 Sevastopol, Russia; kalinskaya@mhi-ras.ru (D.K.); e-shybanov@mail.ru (E.S.)
* Correspondence: hanna.papkova@gmail.com

Abstract: This paper is the first to examine the operation of the HawkEye satellite in the presence of dust aerosol. The study region is the Black Sea. Dust transport dates were identified using visual inspection of satellite imagery, back-kinematic HYSPLIT trajectory analysis, CALIPSO aerosol stratification and typing maps, and the global forecasting model SILAM. In a comparative analysis of in-situ and satellite measurements of the remote sensing reflectance, an error in the atmospheric correction of HawkEye measurements was found both for a clean atmosphere and in the presence of an absorbing aerosol. It is shown that, on average, the dependence of the atmospheric correction error on wavelength has the form of a power function of the form from λ^{-3} to λ^{-9}. The largest errors are in the short-wavelength region of the spectrum (412–443 nm) for the dust and dusty marine aerosol domination dates. A comparative analysis of satellite and in situ measurements of the optical characteristics of the atmosphere, namely the AOD and the Ångström parameter, was carried out. It is shown that the aerosol model used by HawkEye underestimates the Angström parameter and, most likely, large errors and outliers in satellite measurements are associated with this.

Keywords: aerosol optical depth; fine particles; coarse particles; SPM; atmospheric aerosol; dust aerosol; remote sensing; HawkEye; remote sensing reflectance; atmospheric correction; dust; Black Sea; AERONET; Ångström parameter

Citation: Papkova, A.; Kalinskaya, D.; Shybanov, E. Using HawkEye Level-2 Satellite Data for Remote Sensing Tasks in the Presence of Dust Aerosol. *Atmosphere* **2024**, *15*, 617. https://doi.org/10.3390/atmos15050617

Academic Editor: Daren Chen

Received: 6 March 2024
Revised: 12 April 2024
Accepted: 8 May 2024
Published: 20 May 2024

1. Introduction

This study is a continuation of a series of works devoted to the study of the optical properties of atmospheric aerosol over the Black Sea and its influence on satellite data products presented on the Ocean Color platform. A comprehensive analysis of an array of long-term in situ measurements obtained at AERONET (Aerosol RObotics NETwork) stations (NASA), measurement data from the spectrophotometer SPM (Sun Photometer Mobile) and other independent in situ measurements made it possible to complement the understanding of aerosol load in the region under study and the factors that influence it [1–10]. In previous studies, background optical characteristics of atmospheric aerosol were obtained for the Black Sea region: aerosol optical depth at a wavelength of 500 nm AOT(500) = 0.22 ± 0.05 and the value of the Ångström parameter ($\alpha = 1.3 \pm 0.3$ [11]). For the region under study, the influence of background aerosol on the accuracy of remote sensing results is minimal. Theoretical estimates show that the extrapolation error of the aerosol scattering value at wavelength, λ, is proportional to the second-degree polynomial of the wave number $k = 2\pi/\lambda$. The quadratic dependence of errors on k is explained by inaccurate estimates of the contribution of the fine fraction of aerosol particles to radiation scattered by the atmosphere [12–16]. The situation worsens when an aerosol with pronounced absorbing properties appears (smoke, mineral dust, smog, anthropogenic dust) [14,17,18].

Over the Black Sea region, transfers of mineral dust are observed annually both from the African continent (Saharan dust), the Middle East and Asia. Among all types of atmospheric aerosol, it is dust that has the greatest influence on satellite data of the remote sensing reflectance (Rrs(λ)), which, in the presence of an absorbing aerosol, is often negative in the short-wave region of the spectrum (400–443 nm) [2,10,19–24]. Obvious outliers indicate systematic errors in standard atmospheric correction algorithms, which rely on extrapolation of aerosol properties for the visible range from data obtained in the near infra red (NIR) region of the spectrum [25]. Also, a number of studies note the poor performance of standard correction methods for coastal waters, which also manifests itself in negative or overestimated Rrs(λ) values [19,26–28]. These errors mainly occur because the black pixel assumption in the near-infrared (NIR) bands is not valid in turbid waters because of the elevated signals in the NIR bands associated with significant particle scattering. An additional challenge for the NIR-based method is signal saturation over highly reflective waters [29], which further limits the validity of Rrs(λ) products. In Ref. [30], a technique was proposed where two limiting aerosol models are determined for a pixel, then the water reflectance coefficient is calculated by subtracting the signal from the atmosphere (Rayleigh + aerosols) in the entire visible range of the spectrum. Previously, in Ref. [24], it was analytically proven that if there is a dust-absorbing aerosol in the atmosphere above a region, the atmospheric correction error is expressed by a power function of the wavelength of the fourth degree, i.e., close to λ^{-4}. This is due to the absorption by the aerosol of radiation scattered by air molecules (according to Rayleigh's law) $\tau_m^0 \approx \lambda^{-4}$. It can also increase with pronounced spectral properties of aerosol absorption, which are determined by the microphysics of the aerosol (source of dust, processes of its transformation in the atmosphere, etc.). Based on this and the found constancy of the blue color index for the Black Sea, where the ratio Rrs(412 nm)/Rrs(443 nm) is almost always close to 0.8, a correction to the Rrs(λ) values was proposed in Ref. [31]. Later in Ref. [32], it was found that the analytical formula corresponds to the results of numerical calculations of Santinel-3A satellite data using transport theory for cases of intense dust transport over the Black Sea region for 29 November 2021. It was shown that in the range of solar zenith angles 0–55°, the spectral slope of the atmospheric correction error is practically constant, and its analytical expression predicts a value that is overestimated by 0.5. The findings are consistent with the results described in Ref. [33]. When modeling radiative transfer, the authors prove that the effect of absorption prevails over the effect of scattering in the presence of a dust layer when the solar zenith angle approaches 50°. This is due to two factors. Firstly, at lower solar zenith angles, the path length of a direct solar ray through the dust layer is shorter. Secondly, at large solar zenith angles, such as 80°, air molecules located above the dust layer are more effective in reducing the amount of solar radiation reaching the dust layer. Due to strong Rayleigh scattering, especially if the solar zenith angle approaches 80°, the TOA (Top of Atmosphere) albedo is clearly less sensitive to the light scattering properties of dust particles than the reflectivity of the dust layer itself. Conclusions about the absorption of radiation scattered by air molecules by fine dust aerosol, and, as a consequence, the change in the contribution of Rayleigh scattering, are also described and discussed in Refs. [34,35]. The reliability of the analytical and experimental conclusions was confirmed by the validation of satellite (MODIS Aqua) and in situ (AERONET-OC) data over the Black Sea region [36]. For the 49 selected dust transport events, principal component analysis (PCA) was used to estimate the contribution of the first eigenvector. The experimental patterns of the MODIS Aqua satellite data validation error in the presence of a dust aerosol had the form of a power function of the form 90 + 08λ^{-n}, where n = 3.57 ± 0.32. Similar results were obtained for the case of transport of mixed aerosol (burning biomass and mineral dust) over the Black Sea region for 18 October 2017–19 October 2017 according to VIIRS SNPP data [37].

Since the MODIS and VIIRS satellites are older generation remote sensing instruments and have low spatial resolution (750 m^{-1} km), the authors of this study conducted a similar study for the new HawkEye remote sensing instrument (SeaHAWK) and verified its performance in different types of atmospheric aerosols over the Black Sea region. It is worth noting that HawkEye currently has the highest spatial resolution (120 m^{-1} km) of all remote sensing tools presented on Ocean Color. This satellite resolution makes it possible to obtain better results of Rrs(λ) measurements in coastal areas, in particular for AERONET-OC stations located 12–15 nautical miles from the Black Sea coast. This was the reason for choosing HawkEye satellite data to study the optical properties and reconstruct the vertical attenuation of light in Lake Baikal [38]. Another interesting feature of HawkEye satellite data is the use of a completely different approach to atmospheric correction, which is similar to the algorithm used in CZCS [19,39].

The HawkEye sensor has a range set similar to SeaWiFS and is capable of using the standard Gordon and Wang (1994) approach for atmospheric correction. Unfortunately, due to technical problems when launching the satellite into orbit and stabilizing it, the problem of loss of sensitivity in the blue region of the spectrum and the presence of large amounts of illumination with "bright targets" (ground, clouds) arose, which greatly affects the NIR bands [40]. For this reason, using NIR bands for atmospheric correction would inevitably be accompanied by large errors in standard products. To avoid this, one aerosol model is used (instead of the 80 used in the current implementation of the GW94 approach) with the 670 nm band to estimate the aerosol contribution, assuming that the remote sensing reflectance at 670 nm is negligible. The disadvantage of this method is that with a moderate or large contribution from the remote sensing reflectance, this correction will not be effective and the aerosol signal will be overestimated, which will lead to underestimated Rrs(λ) values. The technical characteristics and atmospheric correction of HawkEye will be discussed in more detail in Section 2.

The purpose of this study is to test the quality of HawkEye satellite products for the Black Sea region in the presence of background and absorbing dust aerosol. The analysis is carried out in two stages, the first of which includes consideration of the optical characteristics of the atmosphere on selected dates. The second stage is devoted to the influence of aerosols on the magnitude of atmospheric correction error when calculating the remote sensing reflectance for cases with recording background and dust aerosol in the atmosphere. The magnitude of the error is determined by comparing in situ (AERONET-OC) and satellite data. The work also compared results of in situ measurements (by SPM (MHI RAS) and AERONET)) and satellite AOT data at a wavelength of 870 nm (AOT(870)) and Ångström parameter at wavelength 440–870 nm (α).

It is worth noting that such an analysis for the HawkEye satellite in the presence of mineral dust in the atmosphere was carried out for the first time, which determines the novelty and relevance of this work. Also, comparisons of its satellite measurements with in situ measurements presented on the Ocean Color SeaBASS platform (SeaWiFS Bio-optical Archive and Storage System) have not yet been carried out, which also emphasizes the novelty of the study [41].

2. Materials and Methods

2.1. HawkEye Satellite, Technical Characteristics and Algorithm of Atmospheric Correction

The main remote sensing tool considered in this work is a low-cost miniature ocean color sensor (HawkEye) carried aboard a Cube Sat (SeaHawk). The HawkEye instrument collects images that are 1800 pixels × 6000 lines over 100 s which at the current altitude (~585 km) provides a scene that is approximately 200 km across track and 600 km along track. Schedules for image collection and data downlinks are created to cover a 10-day period (approximately 100 images per week). As noted before, HawkEye uses CZCS correction. The longest available wavelength for CZCS ocean observations is 670 nm, which has a small but significant water-leaving radiance contribution in oligotrophic and mesotrophic waters (larger and less predictable in eutrophic and turbid waters). To determine the water-leaving radiance contribution at 670 nm (and thereby the aerosol contribution at that longest wavelength), the OBPG developed an iteration scheme very similar to Ref. [42]. This was used in combination with an assumption about the aerosol type to determine the aerosol contribution in the shorter visible wavelengths. The CZCS algorithm uses a linear relationship between particulate backscattering and Rrs_550 described in Ref. [43]. The spectral scattering function described by Ref. [44] is used to estimate backscattering at 670 nm from backscattering at 550 nm. The radiance model formulation [45] is then used to estimate reflectance at 670 from backscattering and absorption. The absorption terms account for water (computed a priori for the CZCS spectral bands) particulate matter (estimated from chlorophyll via Ref. [46]), and detritus (estimated via Ref. [42]). This algorithm uses only one aerosol model, namely the aerosol type was fixed to that of a maritime aerosol at 99% relative humidity. This M99 aerosol is one of the most commonly retrieved aerosol types in the global SeaWiFS and MODIS processing. With the aerosol type fixed, and a method developed to estimate water-leaving reflectance at 670 nm (Rrs_670) given water-leaving reflectance at 550 nm (Rrs_550) and chlorophyll (Chl), an iteration process is employed until Rrs_670 stops changing. As a verification of this approach, a time-series was generated using SeaWiFS data processed using (1) the standard NIR algorithm, and (2) the CZCS algorithm (i.e., treating SeaWiFS as if it lacked NIR bands). Comparisons of normalized water-leaving radiance retrievals at 443nm (nLw_443), retrieved chlorophyll, and retrieved vs. modeled nLw_670 are shown below. For this mesotrophic region, the two processing methods yield very similar results. In Ref. [47] it is noted that one possible enhancement to the current OBPG aerosol correction approach would be to utilize a global climatology of aerosol type, such as the SeaWiFS Ångström in situ, to select aerosol type. At the moment, HawkEye uses a fixed value of $\alpha = 0.68420005$. The first image for the Black Sea according to HawkEye dates back to November 2020. It is worth noting that flights of this satellite over the studied region are quite rare; more precisely, during the period 2020–2023, 21 images were obtained for the central and western parts of the Black Sea. For this small data set, detection of dust transport events seemed unlikely, but luck was on the side of the authors.

2.2. In Situ Data, AERONET and AERONET OC Network, Portable Solar Spectrophotometer SPM

AERONET uses automatic photometers (Cimel-318, Cimel Electronique, Paris, France) and standardized procedures for calibration and processing of the received data. This was used as a source of in situ measurements of aerosol optical thickness. The AERONET-Ocean Color (AERONET-OC) extension with support marine applications provides an additional capability to measure the water-leaving radiance. This was used to extract data on the spectral radiance coefficient of the sea [48]. At the moment, only two Black Sea stations provide information on the ocean color according to the measurements of Section-7_Platform (29.45° E, 44.45° N) (in the past: Gloria) and Galata_Platform (28.19° E, 43.05° N) stations. In the current research, we used the daily average data of the Level 2 normalized water radiance LWN, which is considered to have better quality. Level 1.5 includes only cloudiness screening using a series of quality tests, while Level 2 consists of completely cleaned data obtained after calibration and software verification [49]. In the course of the research, the values of LWN(λ) were converted into Rrs(λ) by dividing by the solar constant Fo(λ) [50].

To measure the aerosol optical depth and the Ångström parameter over Sevastopol (MHI RAS (33.15170° E, 44,6150° N)), a portable solar spectrophotometer SPM was used [51]. Air samples to assess PM10 and PM2.5 in the ground layer (80–100 m above sea level) concentrations were collected with a dust analyzer "Atmas" (Moscow, Russia, https://ntm.ru/products/150/8342 [accessed on 5 December 2022]) every day since February 2020 to November 2021 [52]. The analyzer was equipped with an impactor, with replaceable nozzles for fractional separation of suspended aerosol particles (PM10, PM2.5). The "Atmas" directly measured the mass concentration. There was no need to adjust the conversion factor for different dust compositions. The dust analyzer operation principle was based on the piezoelectric measurement method, the essence of which was to measure the in situ frequency of the piezoelectric element during the deposition of aerosol particles on its surface. When the air was pumped through the analyzer, the particles in the air sample entered the corona discharge in situ created by the electrode, where they received an electric charge and were deposited on the surface of the piezoelectric element. When particles were deposited on the surface of the piezoelectric element, the frequency of its oscillations changed, which was proportional to the mass of the settled dust. The measurement range of the mass concentration of dust was 0.1–150 mg m^{-3}. The error in the concentration range from 0.1 to 20 mg m^{-3} was equal to 20%. If the dust concentration was more than 20 mg m^{-3}, it was necessary to use a special diluents cartridge, while the error was ±25%. Single values of the concentration of PM were recorded every 5 s [53].

2.3. Additional Tools for Comparative Analysis and Confirmation of Dust Presence

The sources of aerosol transport can be analyzed using the results of modeling the back trajectories of air flow movement using the HYSPLIT V1 software package (Integrated hybrid Lagrangian trajectory model for a single particle) developed by the Air Resources Laboratory (ARL), (https://www.ready.noaa.gov/HYSPLIT.php [accessed on 21 June 2023]). To confirm the presence of a dust aerosol over the Black Sea, in addition to satellite data and analysis of optical characteristics based on in situ data, the HYSPLIT model data were used [54]. A comprehensive analysis of the described data makes it possible to predict the region of aerosol origin (source) and visualize the stratification of various types of atmospheric aerosols using CALIPSO satellite data [55,56]. Additionally, to confirm the presence of dust, the System for Integrated modeLing of Atmospheric composition (SILAM v.5.7/5.7.1) was used [57,58].

The HawkEye satellite measurements are compared with measurements from another high-resolution satellite, namely OLCI. The Ocean and Land Color Instrument (OLCI) installed aboard Sentinel 3A, and Sentinel 3B is a European Space Agency Earth observation satellite dedicated to oceanography that launched on 16 February 2016. The Ocean and Land Color Instrument (OLCI) is the successor to ENVISAT's Medium Resolution Imaging Spectrometer (MERIS), having additional spectral bands, different camera arrangements, and simplified onboard processing. The OLCI is a push-broom instrument with five camera modules sharing the in situ view. The in situ of view of the five cameras is arranged in a fan-shaped configuration in the vertical plane, perpendicular to the platform velocity. Each camera has an individual in situ view of 14.2° and a 0.6° overlap with its neighbors. The whole in situ view is shifted across the track by 12.6° away from the sun to minimize the impact of sun glint. OLCI is equipped with onboard calibration hardware based on sun diffusers. There are three sun diffusers: two "white" diffusers for radiometric and one for spectral calibration, with spectral reflectance features. The native resolution is approximately 300 m, referred to as Full Resolution (FR). A Reduced Resolution (RR) processing mode provides Level-1B data at sampling rates decreased by a factor of four in both spatial dimensions resulting in a resolution of approximately 1.2 km [59].

3. Results and Discussion

The optical characteristics of the atmosphere for the period since 2021 to 2023 which include 21 days of HawkEye satellite data obtained for the Black Sea region are the main research results. The data are presented for the western and central parts of the Black Sea. As mentioned above the HawkEye validation data is not available in the SeaBASS database. This means that a similar procedure was used to correct satellite data in the SeaDAS V. 7.5.3. software package. Satellite measurements were averaged for an area (5 km × 5 km) centered above the in situ measurement site. The satellite value is defined as the average Rrs(λ) value not marked with error flags pixels. Spatial homogeneity and the proportion of pixels with error flags are also evaluated. All pixels containing the following error flags were excluded: LAND, glint (STRAYLIGHT, HIGLINT, HILT, MODGLINT, ATMWAR) and navigation errors (NAVFAILE), cloud boundaries or ice (CLDICE) and underestimated Lwn (LOWLW). The quality of satellite images is influenced by the geometry of observations, especially in the case of dust aerosol presence [33]. Consequently, the data with error flags HISOLZEN (large values of the zenith angle of the sun) and HISATZEN (high values of the sensor observation zenith angle) were additionally removed. This corresponds to the protocols for comparing and improving the quality of data from both NASA and

NOAA [60,61]. After data correction for the selected pixels, 11 images were received (28 May 2021, 26 July 2021–28 July 2021, 17 August 2021, 26 September 2021, 5 November 2021, 17 February 2022, 2 April 2022, 25 April 2022, 17 May 2022). Since the averaging of satellite pixels was centered on two AERONET Black Sea stations, only 14 measurements were left: 9 for Galata_Platform and 5 for Section_7. Unfortunately, not all HawkEye images covered 2 stations at the same time and also not all days showed a complete absence of clouds, straylight or other error flags. Despite all the steps described for satellite data rejection, data with negative values of the remote sensing reflectance in the short-wavelength spectrum range remained. Also, despite the high degree of data selection, days with suspected dust in the atmosphere over the researched region remained. For such days, the analysis of the in situ and satellite data variability was continued.

The first stage of the study contains an analysis of full-scale measurements of the atmosphere optical characteristics over the Black Sea AERONET stations and photometric SPM in-situ measurements received in Sevastopol on the dates under study. Conclusions about the presence of dust in the atmosphere over the Black Sea were based on satellite data and additionally from high values of AOD and low values of the Ångström parameter. Low values of AOD (AOD(500) < 0.1) are observed in a clean atmosphere, and values of $\alpha > 2$. We planned to use the "Atmas" dust meter to analyze the fine and coarse dispersed fractions of aerosol in the ground layer (100 m above sea level). Unfortunately, the return trajectories of HYSPLIT did not confirm the transfer specifically from the Sahara, and we decided not to add this data to avoid errors and uncertainties. Table 1 shows measurements of AOD and α for the obtained dates at four wavelengths: 412 nm, 443 nm, 510 nm and 865 nm, as well as the Ångström parameter at wavelengths 440–870 nm. Additionally, the predominant radius of aerosol particles based on the inversion products of AERONET V3 [62] was determined. The average daily values were considered at the highest level of data processing quality (level 2).

As was mentioned above, the background atmosphere aerosol values for the Black Sea region are AOD(500) = 0.22 ± 0.05; $\alpha = 1.3 \pm 0.3$, so, from Table 1 it can be assumed that on 2 April 2022, 25 April 2022, 17 February 2022, 5 November 2021, 27 July 2021–28 July 2021 mineral dust was present in the atmosphere. For 28 May 2021, 26 July 2021, 17 August 2021, 26 September 2021 and 17 May 2022, low AOD values (AOD < 0.22) and average values of the Ångström parameter ($\alpha > 1.3$) were obtained, which means that these days can be denoted as relatively "clean" days (the main optical characteristics are close to background values). For the selected dates, analysis of System for Integrated Modeling of Atmospheric composition (SILAM mode l.5.7/5.7.1) [57] was performed to determine the concentration of PM2.5 and PM10 particles to state the presence or absence of dust in the atmosphere. According to SILAM data, dust plumes and high concentrations of coarse PM10 particles (40–80 mg/m^3) over the western and central part of the Black Sea were identified on 2 April 2022, 25 April 2022, 17 February 2022, 5 November 2021. By SILAM modeling data for 28 July 2021, the average concentrations of fine and coarse particles (<25 mg/m^3) were obtained over the western part of the Black Sea. For the selected dates, the next stage of the study is the analysis of atmospheric aerosol stratification maps by CALIPSO satellite data [63]. For this task the latest version of the CALIPSO V4 typing algorithm was used [64]. Over the eastern part of the Black Sea on 28 May 2021 at an altitude up to 5 km, marine and polluted marine aerosols were observed, and at an altitude of 8 km, the smoke aerosol was registered. On 27 July 2021, the polluted marine and polluted continental aerosols were registered at an altitude up to 2 km. The marine and dusty marine aerosols were registered on 26 September 2021 and 17 August 2021 at an altitude up to 2 km. The dust aerosol and polluted dust aerosol were observed on 17 February 2022, 2 April 2022 and 25 April 2022 over the central and western part of the Black Sea at an altitude up to 5 km.

Table 1. Daily and monthly aerosol optical depth and Ångström parameter measurement averages for each date.

Data	Station	AOD (412)	AOD (443)	AOD (510)	AOD (865)	α	PM
28 May 2021	Galata	0.282	0.255	0.210	0.103	1.386	-
	Section_7	0.245	0.226	0.19	0.111	1.068	-
			AOT(441)	AOT(501)	AOT(872)		
	MHI		0.197	0.177	0.165	0.632	
26 July 2021	Galata	0.252	0.225	0.179	0.070	1.780	fine
	Section_7	0.267	0.236	0.19	0.077	1.724	fine
27 July 2021	Galata	0.266	0.247	0.215	0.134	0.979	coarse
	Section_7	0.267	0.243	0.208	0.118	1.111	coarse
28 July 2021	Galata	0.304	0.284	0.252	0.170	0.783	coarse
	Section_7	0.343	0.317	0.279	0.177	0.887	coarse
17 August 2021	Galata	0.111	0.099	0.081	0.032	1.742	fine
	Section_7	0.12	0.106	0.089	0.039	1.576	fine/coarse
26 September 2021	Galata	0.132	0.119	0.095	0.042	1.560	coarse
	Section_7	0.134	0.119	0.098	0.044	1.545	fine/coarse
5 November 2021	Galata	0.084	0.08	0.071	0.049	0.751	coarse
	Section_7	0.152	0.145	0.131	0.087	0.818	coarse
	MHI		0.075	0.065	0.059	1.006	
17 February 2022	Galata	0.28	0.268	0.243	0.181	0.600	coarse
	Section_7	0.283	0.270	0.246	0.175	0.667	coarse
	MHI		0.259	0.246	0.237	0.366	
2 April 2022	Galata	0.151	0.146	0.134	0.108	0.488	coarse
	Section_7	0.073	0.067	0.06	0.036	0.989	-
	MHI		0.204	0.193	0.187	0.361	
25 April 2022	Galata	0.221	0.209	0.185	0.137	0.667	coarse
	Section_7	0.193	0.178	0.143	0.104	0.966	coarse
	MHI		0.101	0.088	0.080	0.924	
17 May 2022	Galata	0.234	0.209	0.166	0.074	1.560	fine
	Section_7	0.364	0.326	0.263	0.114	1.594	fine
	MHI		0.296	0.248	0.215	1.512	

The next step of research is the complex analysis of VIIRS satellite images (Figure 1) and HYSPLIT model 7-day back trajectories for the selected dates (Figure 2). Because the HawkEye satellite regularly flies over the Black Sea region within 8.30–9 a.m. the modeling of trajectories were made for 9 a.m. with AERONET-OC stations communication. The analysis of these data makes it possible to more reliably conclude the source of the aerosol. For example, if the movement at any height was over the desert, then a dust aerosol is more likely to be registered over the researched region [65].

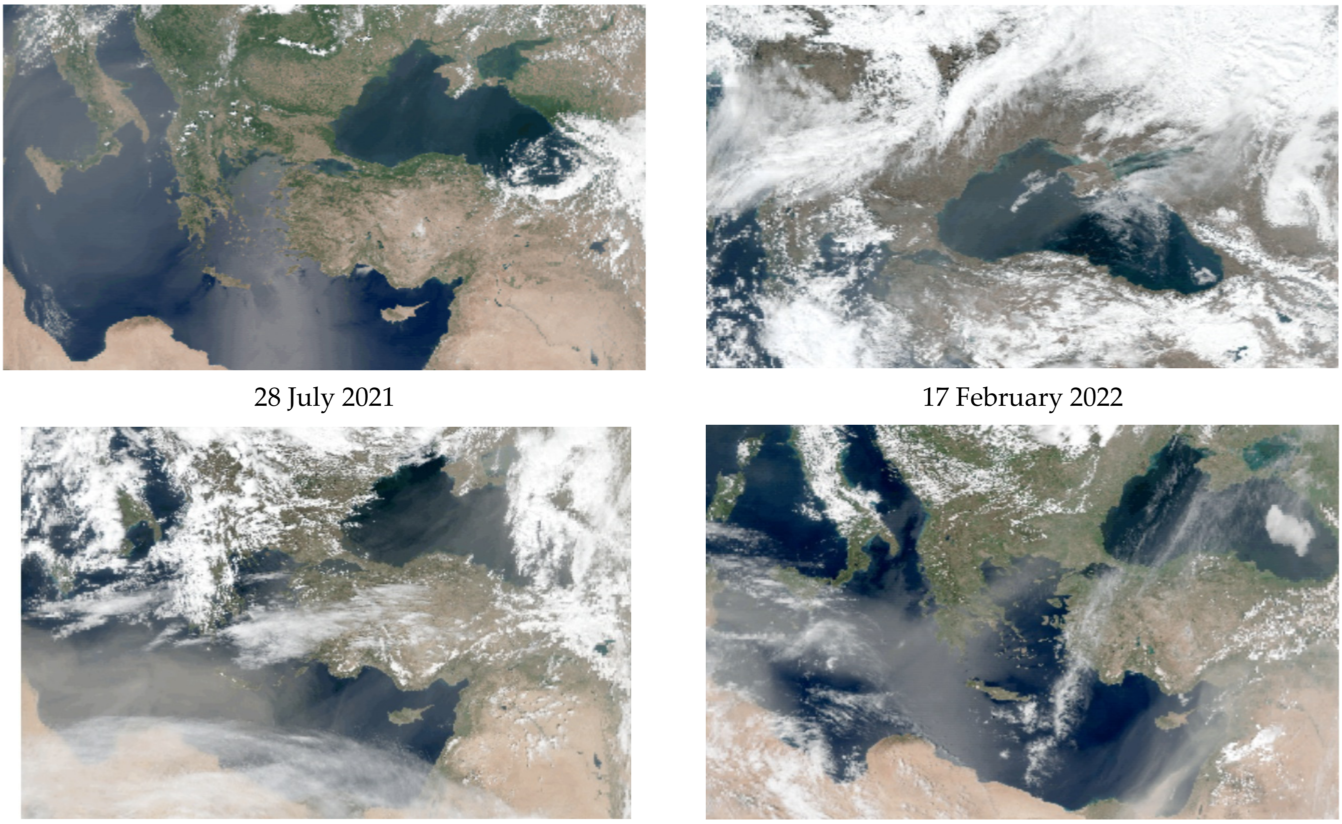

Figure 1. Satellite images of QuasiTrueColor VIIRS for the studied dates (source: https://oceancolor.gsfc.nasa.gov/ [accessed on 15 April 2023]).

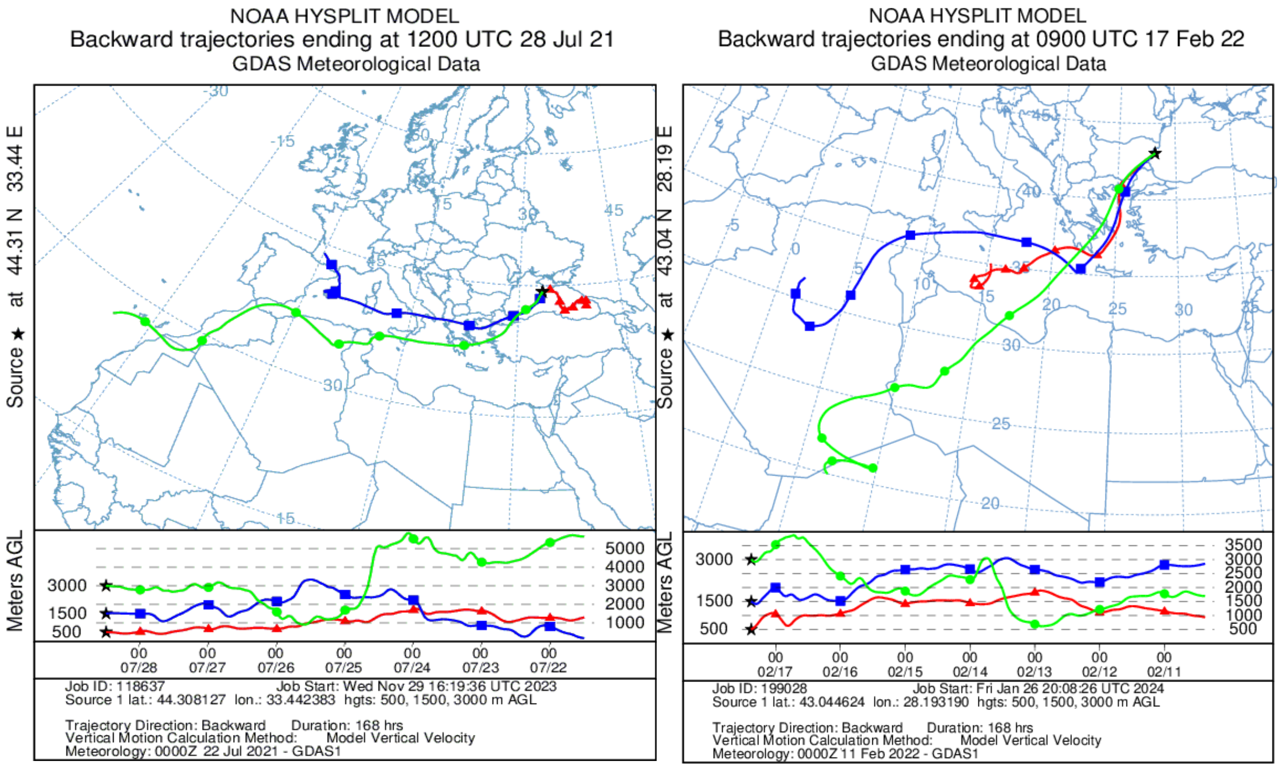

Figure 2. *Cont.*

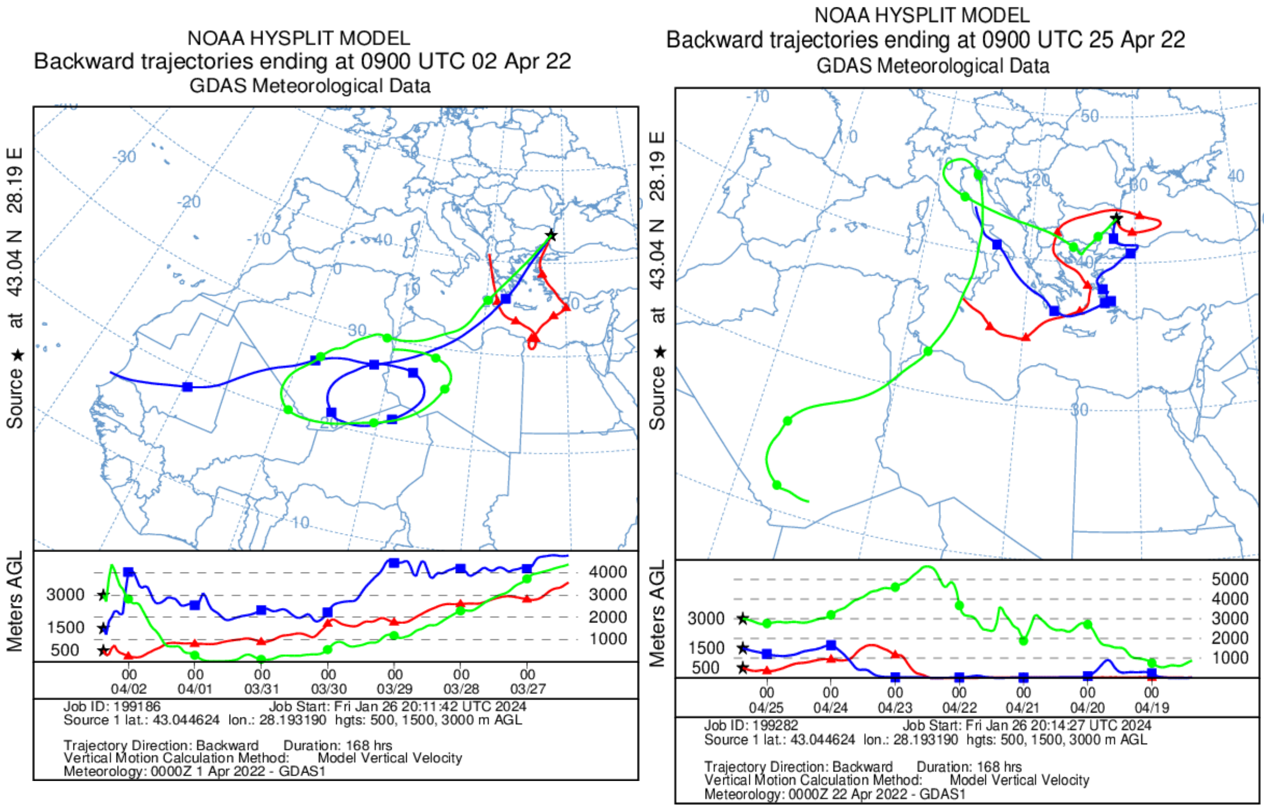

Figure 2. The HYSPLIT 7-day back trajectories of airflow for the Black Sea region.

According to satellite images, dust air flow movements were confirmed on 27 July 2021 (afternoon), 28 July 2021, 17 February 2022, 2 April 2022 that were visualized as plumes of white or yellow color mainly from the south-west direction (Figure 1). Over the Black Sea region on 5 November 2021, heavy clouds were observed so it is not possible to confirm or deny the presence of dust from the images but based on the back trajectories, the movement was from Sahara Desert. No anomalies were observed on satellite images for the rest of the selected dates, but sometimes a slight cloud cover was present. Figure 2 confirms that for the selected days, the source of the aerosol is the Sahara Desert.

The next stage of the research is the analysis of full-scale remote sensing reflectance measurements obtained at the western Black Sea AERONET-OC stations, and further comparative analysis of the HawkEye satellite data. It must be noted that before comparing the data, it is necessary to interpolate full-scale measurements for the same wavelengths at which the Rrs(λ) satellite data are provided. For the HawkEye, the Rrs(λ) measurements are carried out at λ = 412 nm, 447 nm, 488 nm, 510 nm, 556 nm and 670 nm, and for the AERONET Galata_Platform and Section_7 stations, the nearest satellite channels are 412 nm, 443 nm, 488 nm, 510 nm, 560 nm and 667 nm. Despite the slight difference in the channel wavelengths, an improved approach was used in this study to increase the accuracy of interpolation. The problem of remote sensing reflectance values interpolation arises due to the complex shape of the seawater absorption spectrum. Scattering also affects the shape of the Rrs(λ) spectrum. However, the corresponding spectral dependencies do not have sharp jumps, which makes it possible to use a second-degree polynomial for the interpolation. For the Black Sea, the absorption spectrum should be separately distinguished by the absorption of pure seawater, the values of which strongly change the values of Rrs(λ) in the long-wavelength spectrum range. This means that pure seawater absorption is the most inconvenient function for interpolation. Our method involves multiplying the in situ remote sensing reflectance by the value of the seawater model absorption:

$$a_w(\lambda_i) = a_{pw}(\lambda_i) + 0.1 \cdot C_y \cdot \exp[0.015 \cdot (400 - \lambda_i)] \quad (1)$$

where the C_y value is estimated by statistical relationship with the color index:

$$C_y = 2.3 \cdot CI(555/510)^{2.18} \quad (2)$$

The equation was obtained based on the regression dependencies given in Refs. [66,67]. After multiplying the full-scale Rrs(λ) by the model value of the absorption coefficient, the result was interpolated for the satellite channel values by a second-degree polynomial. Then, at the satellite wavelengths, the ratio of the obtained values to the value of the model value of the absorption coefficient was calculated. The next step is a comparison of in situ (and satellite optical characteristics of the atmosphere, namely aerosol optical depth at wavelength 870 nm (AOD(870)) and the Ångström parameter at wavelengths 440 nm and 870 nm (α). The "description" column provides brief day-to-day information based on AERONET, SPM, CALIPSO, SILAM data and analysis of HawkEye satellite images (Table 2). It is noteworthy that all satellite pixels examined within a radius of 5 km from AERONET-OC stations averaged after the cleaning procedure (Section 2). The result of pixel culling based on error flags for some dates resulted in a smaller quantity of data remaining. The main reasons for poor measurement quality were glint and cloudiness. In Table 2, the "Quality" column presents the percentage of high-quality pixels after the culling (filtering) procedure. Unfortunately, the percentage of quality data after this filtering at 5 November 2021, 17 February 2022 and 17 May 2022 was only 1–2%. The most reliable images were obtained on 27 July 2021, 17 August 2021, 26 September 2021, 25 April 2022, 26 July 2021 and 2 April 2022 (AERONET station Section 7). Constructing a linear regression for the AOD values obtained an equation: AOD_HawkEye = 1.215 (AOD_AERONET), with R^2 = 0.69. This indicates a satisfactory correlation between satellite and in situ data with a regular overestimation of satellite AOD values. The value of the Ångström parameter α = 0.6842, obtained from the M99 model, is 1.5 to 2.5 times less than the measured in situ α value, which indicates that its use for this region is incorrect.

Further in this work an analysis of errors in the satellite and in situ data validation was carried out, namely the calculation of the difference between Rrs(λ)AERONET) and Rrs(λ) (HawkEye) (Table 3). It was shown that for those dates when the α was overestimated and the presence of a dust aerosol was not identified, the overestimated Rrs(λ) values were obtained at all spectral wavelengths. On the contrary, on days with the presence of mineral dust in the atmosphere when the values of α_HawkEye (α_H) and α_Aeronet (α_A) differed minimally, the remote sensing reflectance values were underestimated at all wavelengths of the spectrum by the HawkEye data. Interesting results were obtained for days when the predominant aerosol type according to CALISPO data was identified as dust-marine (polluted marine) aerosol. This type of aerosol has both scattering properties that are strongly dependent on wavelength, and, based on its chemical composition, absorbing properties. The sign of the difference between Rrs(λ) (AERONET) and Rrs(λ) (HawkEye) was variable, depending on the wavelength. For clarity, on Figure 3, the examples of satellite and in situ Rrs(λ) spectra for the cases of various types of atmospheric aerosol are presented.

Table 2. In situ and HawkEye comparison of AOD and α data for the researched dates with a brief summary of the day.

Date and Station	AOT(867)_H	AOT(865)_A	α_H	α_A	Quality %	Description
28 May 2021 Galata	0.1255	0.103	0.6842	1.386	53	Low α, low aerosol load, marine polluted aerosol, cloud cover
27 July 2021 Galata	0.1074	0.134	0.6842	0.979	62	AOD and α are slightly overestimated, Polluted marine + continental + dust aerosol, haze
28 July 2021 Galata	0.1634	0.170	0.6842	0.783	16	Slightly overestimated α, dust aerosol
17 August 2021 Galata	0.0485	0.032	0.6842	1.742	60	α is underestimated by 2.5 times, polluted dust and clean marine aerosol
26 September 2021 Galata	0.0822	0.042	0.6842	1.560	65	AOD is underestimated by 2 times, α is overestimated by 2 times, polluted marine aerosol
5 November 2021 Galata	0.0614	0.049	0.6842	0.751	1	AOD is slightly underestimated, α is slightly overestimated, cloud cover, dust aerosol
17 February 2022 Galata	0.2469	0.181	0.6842	0.600	2	The AOD is greatly overestimated, cloud cover, the presence of dust aerosol and polluted dust
2 April 2022 Galata	0.1034	0.108	0.6842	0.488	16	Slightly overestimated α, dust aerosol
25 April 2022 Galata	0.1504	0.137	0.6842	0.667	85	AOD is slightly overestimated, dust aerosol, cloud cover
26 July 2021 Section_7	0.1075	0.077	0.6842	1.545	63	α is underestimated by 2.5 times, the presence of fine polluted marine aerosol particles
27 July 2021 Section_7	0.1062	0.118	0.6842	1.111	25	The α is underestimated, the presence of a marine and dust aerosol
17 February 2022 Section_7	0.2473	0.175	0.6842	0.667	27	Overestimated AOD, dust aerosol
2 April 2022 Section_7	0.0699	0.036	0.6842	0.989	53	Overestimated AOD, understated α, dusty, cloudy
17 May 2022 Section_7	0.219	0.114	0.6842	1.594	2	AOD is overestimated by 2 times, α is underestimated by 2.5 times, fine aerosol

Table 3. HawkEye data validation error for the Black Sea region for the obtained dates.

Data/Rrs(λ)	412 nm	447 nm	490 nm	510 nm	556 nm	670 nm	Slope	R^2
28 May 2021 Galata	−0.00306	−0.00245	−0.00094	−0.00098	−0.00122	0.000193	−5.260	0.916
27 July 2021 Galata	−0.00014	−0.00145	−0.00091	−0.00073	−0.00082	0.000207	−1.481	0.125
28 July 2021 Galata	0.003183	0.000248	0.001139	0.000845	0.001018	0.000325	−7.017	0.609
17 August 2021 Galata	0.001112	−0.0009	7.86×10^{-6}	−0.00046	−0.00049	0.000138	−9.457	0.134
26 September 2021 Galata	0.000497	−0.00152	-4.3×10^{-5}	-2.3×10^{-5}	0.000481	0.000394	−4.395	0.023
5 November 2021 Galata	0.004687	0.002371	0.003015	0.002984	0.002297	0.000519	−2.774	0.783
17 February 2022 Galata	0.003343	0.002139	0.000762	0.000839	−0.00111	2.74×10^{-5}	−8.837	0.825
2 April 2022 Galata	0.001837	0.00039	0.000887	0.00102	0.001232	0.000643	−1.582	0.244
25 April 2022 Galata	0.002529	0.000254	0.000446	0.000354	0.000644	0.000562	−9.457	0.702
26 July 2021 Section_7	−0.00284	−0.00185	-8.8×10^{-5}	0.000172	−0.00035	7.44×10^{-5}	−9.457	0.905
27 July 2021 Section_7	0.001592	−0.00062	0.000546	0.000737	0.001001	0.000819	0.325	0.003
17 February 2022 Section_7	0.004708	0.000261	−0.00077	−0.00149	−0.00156	6.95×10^{-5}	−9.457	0.552
2 April 2022 Section_7	0.00048	−0.00127	0.000408	−0.00025	0.001001	0.000613	3.457	0.126
17 May 2022 Section_7	−0.00519	−0.00559	−0.00348	−0.00254	−0.0019	0.000534	−3.931	0.836

As can be seen from Table 3, the greatest difference between the data is observed on channels in the short-wavelength spectrum range (412–447 nm) and at a wavelength of 556 nm. The smallest differences were observed at 490 nm, 510 nm and 670 nm. In the cases of a dust aerosol presence, the difference between in situ and remote sensing reflectance in the short-wave spectrum range has the highest positive value. To approximate the error in Rrs(λ) values determined by a power law, a nonlinear optimization method was used. The need to use a nonlinear optimization method is due to the presence of a variable sign in the difference of the Rrs(λ)spectral values from in situ and satellite data. In this work, by analogy with Ref. [68], we use the residual (*SSE*—sum of square error) as the initial function:

$$SSE = \sum_{i=1}^{n} \left[Rrs_{field} - Rrs_{sat} - \delta_{400} \cdot (\lambda/400)^{\gamma} \right]^2 \quad (3)$$

At the same time, there are two unknowns in the equation: δ_{400}—deviation in the shortwave region and γ—exponent. The value δ_{400} is found by differentiating Equation (1), for any γ value. Thus, the task reduced to a numerical search of a one-variable function minimum. To characterize the tightness of the connection, a regression ratio was calculated:

$$R^2 = \sum_{i=1}^{n} \left[\delta(\lambda) - \delta_{aprox}(\lambda) \right]^2 / \sum_{i=1}^{n} \left[\delta(\lambda) - \overline{\delta} \right]^2 \quad (4)$$

Low values are quite common in Table 3, which indicates that there is no obvious pattern in the difference between in situ and satellite data. A positive validation error simultaneous with high R^2 values were observed at the AERONETGalata_Platform station on 28 July 2021, 5 November 2021, 17 February 2022 and 25 April 2022. According to

Table 2, the minimum difference between in situ and satellite values corresponds to this. Large values of validation error with a negative sign are observed on 28 May 2021 at the Galata_Platform station, as well as on 26 July 2021 and 17 May 2022 at Section_7 stations, while the Ångström parameter had values two or more times higher than the model value 0.6842, and the values of AOD(865) are in the range of 0.077–0.114. At lower values of AOD(865) the error decreases, which is explained by a decrease in the contribution of the atmosphere to the total signal at TOA.

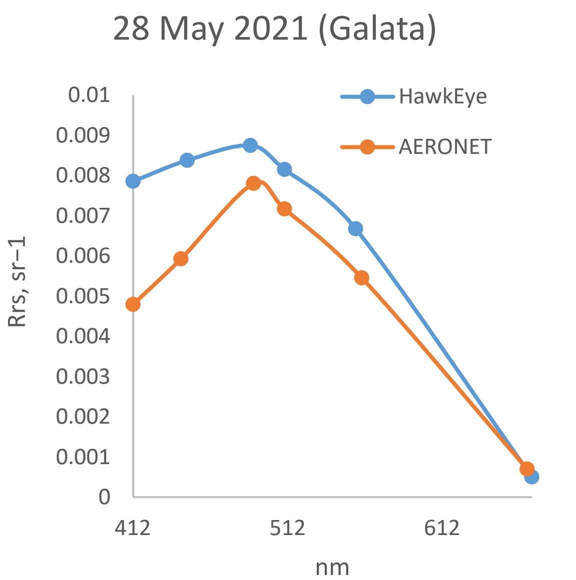

(**a**)

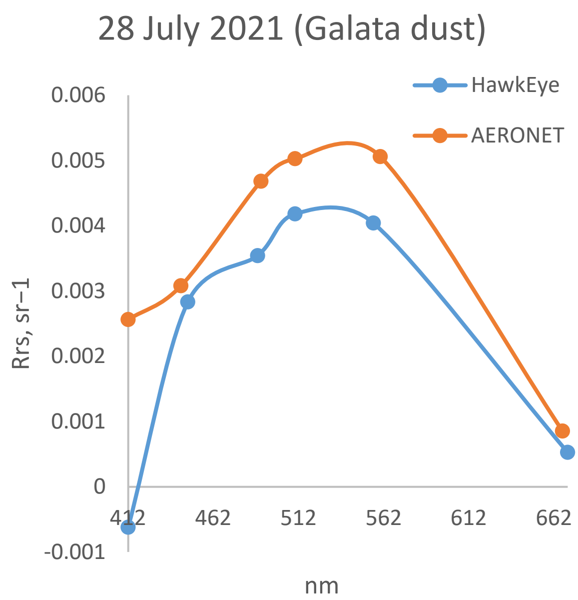

(**b**)

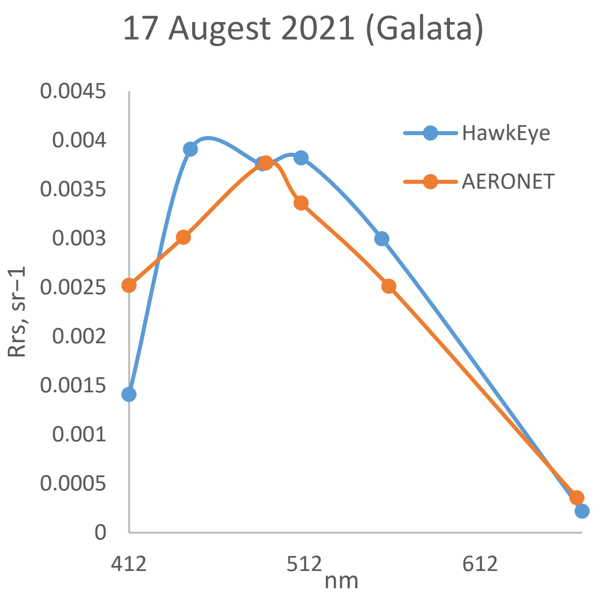

(**c**)

Figure 3. In situ and satellite values of Rrs(λ) for (**a**) 28 May 2021 (clear excess of satellite Rrs(λ)), (**b**) 28 July 2021 (dust aerosol with low satellite Rrs(λ)), (**c**) 17 August 2021 (satellite Rrs(λ) overestimated or underestimated).

4. Discussion

From Tables 2 and 3 it can be seen that satellite Rrs(λ) in the shortwave region and 556 nm contain large errors not only on dust transfer days, but also in the presence of background aerosol. It was shown that for dates without dust transport, the α values were overestimated (the dominance of fine mode aerosols), and the values of Rrs(λ) were overestimated on all spectral channels. On the contrary, on days with the presence of mineral dust in the atmosphere, when the values of α_H and α_A almost coincide, the HawkEye remote sensing reflectances were underestimated. On the days with the identification of the dust-marine aerosol, when the greatest errors were observed in the shortwave region and at 556 nm, the data at 470 nm and 670 nm had a smaller deviation, which corresponds to the principle of the atmospheric correction algorithm operation for HawkEye. With nonlinear optimization of HawkEye atmospheric correction errors, it is seen that with a dust aerosol, the power dependence is expressed by a degree from λ^{-3} to λ^{-9}. Most often, such a steep course of the power function is associated with underestimated satellite values of the remote sensing reflectance of the sea at the wavelength 412 nm.

The authors of this research suggest that the main problem of incorrect HawkEye satellite data for the Black Sea is in an incorrect estimate of the Ångström parameter. It is noted in Ref. [47] that one possible enhancement to the current OBJECT aerosol correction approach would be to utilize a global climatology of aerosol type, such as the SeaWiFS Ångström in situ, to select aerosol type. Nowadays, a fixed value α = 0.68420005 is used for HawkEye according to the M99 aerosol model (aerosol type was fixed to that of a maritime aerosol at 99% relative humidity). From Table 2, it can be seen that in most of the presented dates, this value is greatly overestimated. That is why a long-term array of in situ data was additionally analyzed based on the results of AERONET and SPM measurements. For the Section_7 station, the 1067 values of α were analyzed, which allowed us to determine the average value of α = 1.39 ± 0.32. For the Galata_Platform station, the 2074 values was averaged and the result is α = 1.47 ± 0.34. According to the SPM data, the analysis of measurements was carried out for 834 days (2970 measurements) and the average value of the Ångström parameter for this data is α = 1.13 ± 0.26.

As a result, it was concluded that fixing the α = 0.68 value is not advisable, because the average of the Ångström parameter values for the Black Sea region ranges from 1.1–1.5. Values below and equal to 0.68 have only 4–7% of the data. We suppose that this is the reason why even with a relatively clean atmosphere over the Black Sea region, the satellite values of the HawkEye remote sensing reflectance contain large errors. It is worth noting that when choosing a fixed value of the α, it is necessary to rely on in situ data, and not on the data from other satellites. In the long-term analysis of satellite data, mainly Modis Aqua, VIIRS NOAA, Santinel 3B and Santinel 3A are used to determine the hydrophysical and optical characteristics of the water. The listed satellite data are available in the SeaBASS [69] database, and have a very wide range (Figure 4) and a tendency to underestimate the α values.

In the presence of a dust aerosol in the atmosphere, especially in the spring period, the Ångström parameter is close to a fixed value of α = 0.68, however, the dust and its extinguishing properties alone contribute the main errors when the Rrs(λ) is determined by the HawkEye satellite measurements. Therefore, in order to improve the quality of HawkEye satellite products, a regional recalculation of the model fixed values of α is necessary. In this paper for the Black Sea region the calculation was made based on the condition that α = 1.28, which is 2 times higher than that used by the M99 model.

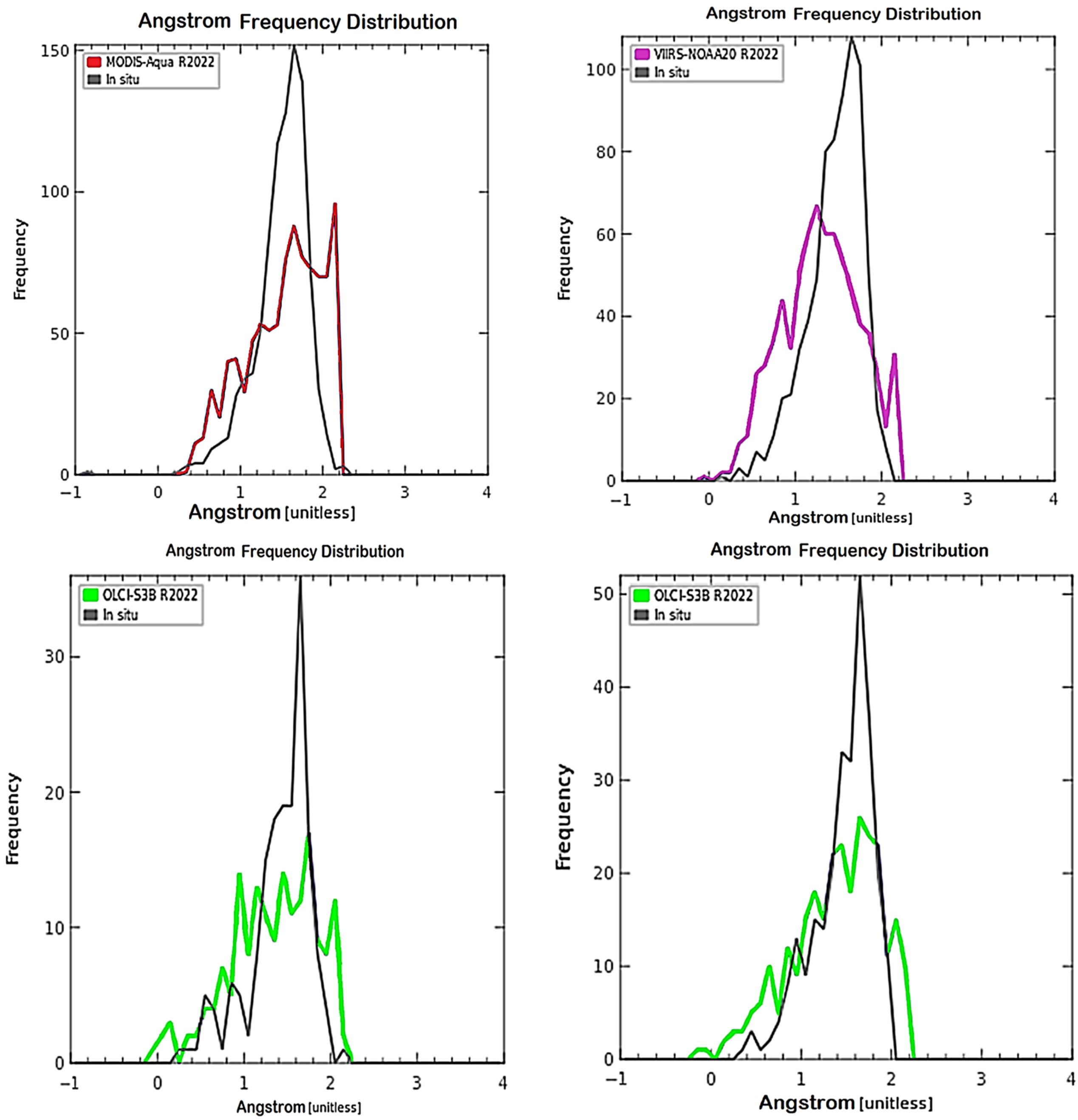

Figure 4. Frequency distribution of satellite and in situ AERONET-OC stations values of the Ångström parameter for the Black Sea region.

The authors evaluated the accuracy of the Ångström parameter determining for the case of coincidence of two new high-resolution satellites HawkEye and Sentinel 3A/3B measurements. It was shown in Ref. [70] that OLCI Sentinel presents highly accurate results for the Black Sea, in particular for the coastal zone. For example, on 28 May 2021 in the case of the regional background aerosol presence (Table 2), when $\alpha = 1.39$ was obtained at the AERONET Galata_Platform station, for the same date according to HawkEye data, this value was 2 times lower, and according to Sentinel 3A measurements, the data were more realistic and closer to in situ data ($\alpha = 1.123$). It can be seen from Figure 5 that the satellite remote sensing reflectance spectrum by Sentinel 3A measurements has great consistency with the in situ data. A similar situation was observed for 25 April 2022 and 17 May 2022.

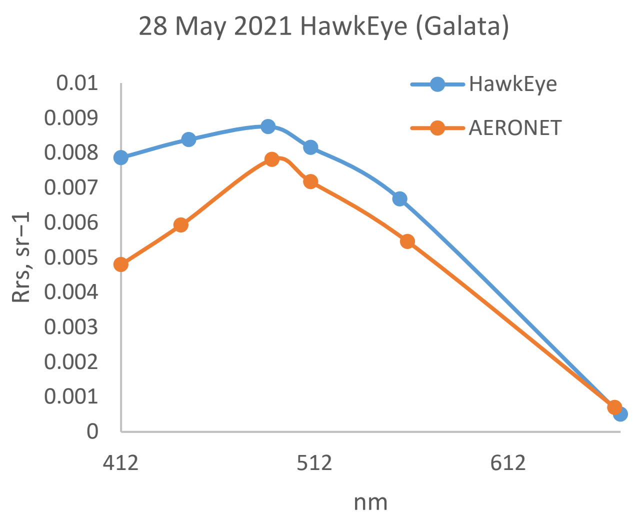

(a)

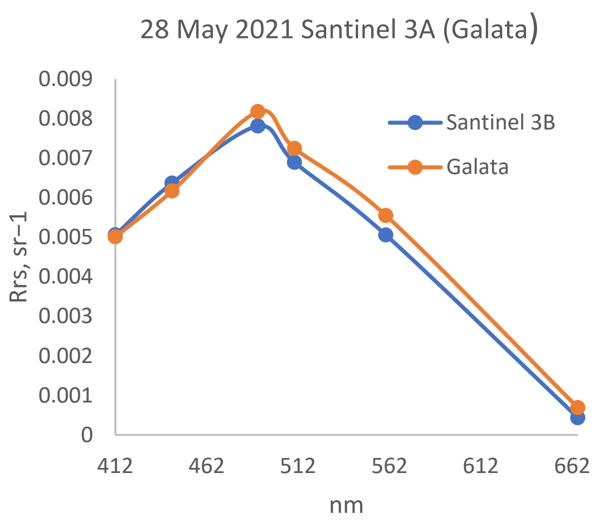

(b)

Figure 5. Remote sensing reflectance on 28 May 2021 for Galata_Platform station according to HawkEye (**a**) and Sentinel 3A (**b**) data.

From Figure 5 it can be seen that for HawkEye, it is necessary to take into account the regional background values of α. It may be advisable to use this approach not only for the Black Sea region, but also for other water areas where in situ α data with good spatial and temporal resolution are available.

Author Contributions: Conceptualization, A.P., E.S. and D.K.; validation, E.S., D.K. and A.P.; data curation, A.P. and E.S.; writing—original draft preparation, D.K. and A.P.; writing—review and editing, D.K. and A.P.; project administration, A.P. All authors have read and agreed to the published version of the manuscript.

Funding: The research is made in the framework of the topic of the state task of the Marine Hydrophysical Institute RAS FNNN-2024-0012 "Analysis, diagnosis and operational forecast of the state of hydrophysical and hydrochemical fields of marine waters based on mathematical modeling using data from remote and contact measurement methods ("Operational Oceanology")".

Institutional Review Board Statement: Not applicable.

Informed Consent Statement: Not applicable.

Data Availability Statement: Satellite and AERONET data available in a publicly accessible repository that does not issue DOIs. SPM data presented in this study are available on request from the Kalinskaya D.V. The data are not publicly available due to privacy concerns.

Acknowledgments: The authors thank Tom Kucsera, Brent Holben, Giuseppe Zibordi and Gene Feldman's group from NASA for the pre-delivery of AOD data, calculations of BTA data, processing of measurements obtained at the Sevastopol AERONET station, and for the possibility of using high-quality photometric measurement data. The authors also express their gratitude to Sakerin S.M. and Kabanov D.M. for providing the SPM photometer and its software. The CALIOPV4.10 data were obtained from the NASA Langley Research Center Atmospheric Science Data Center at https://asdc.larc.nasa.gov/project/CALIPSO [accessed on 13 December 2023]. The authors provide acknowledgement to NASA Ocean Biology Distributed Active Archive Center (OB.DAAC) for the use of data, imagery, and web resources for educational and informational purposes.

Conflicts of Interest: The authors declare no conflict of interest.

References

1. Kabashnikov, V.; Milinevsky, G.; Chaikovsky, A.; Miatselskaya, N.; Danylevsky, V.; Aculinin, A.; Kalinskaya, D.; Korchemkina, E.; Bovchaliuk, A.; Pietruczuk, A.; et al. Localization of aerosol sources in East-European region by back-trajectory statistics. *Int. J. Remote Sens.* **2014**, *35*, 6993–7006. [CrossRef]
2. Kalinskaya, D.V.; Papkova, A.S. Why Is It Important to Consider Dust Aerosol in the Sevastopol and Black Sea Region during Remote Sensing Tasks? A Case Study. *Remote Sens.* **2022**, *14*, 1890. [CrossRef]
3. Ozdemir, E.; Tuygun, G.T.; Elbir, T. Application of aerosol classification methods based on AERONET version 3 product over eastern Mediterranean and Black Sea. *Atmos. Pollut. Res.* **2020**, *11*, 2226–2243. [CrossRef]
4. Suslin, V.; Slabakova, V.; Kalinskaya, D.; Pryakhina, S.; Golovko, N. Optical Features of the Black Sea Aerosol and the Sea Water Upper Layer Based on In Situ and Satellite Measurements. *Phys. Oceanogr.* **2016**, *1*, 20–32.
5. Papkova, A.; Papkov, S.; Shukalo, D. Prediction of the Atmospheric Dustiness over the Black Sea Region Using the WRF-Chem Model. *Fluids* **2021**, *6*, 201. [CrossRef]
6. Korchemkina, E.N.; Kalinskaya, D.V. Algorithm of Additional Correction of Level 2 Remote Sensing Reflectance Data Using Modelling of the Optical Properties of the Black Sea Waters. *Remote Sens.* **2022**, *14*, 831. [CrossRef]
7. Stefan, S.; Voinea, S.; Iorga, G. Study of the aerosol optical characteristics over the Romanian Black Sea Coast using AERONET data. *Atmos. Pollut. Res.* **2020**, *11*, 1165–1178. [CrossRef]
8. Ştefănie, H.I.; Radovici, A.; Mereuță, A.; Arghiuș, V.; Cămărășan, H.; Costin, D.; Botezan, C.; Gînscă, C.; Ajtai, N. Variation of Aerosol Optical Properties over Cluj-Napoca, Romania, Based on 10 Years of AERONET Data and MODIS MAIAC AOD Product. *Remote Sens.* **2023**, *15*, 3072. [CrossRef]
9. Osgouei, P.E.; Roberts, G.; Kaya, S.; Bilal, M.; Dash, J.; Sertel, E. Evaluation and comparison of MODIS and VIIRS aerosol optical depth (AOD) products over regions in the Eastern Mediterranean and the Black Sea. *Atmos. Environ.* **2022**, *268*, 118784. [CrossRef]
10. Suetin, V.S.; Korolev, S.N.; Suslin, V.V.; Kucheryavy, A.A. Manifestation of features of the optical properties of atmospheric aerosol over the Black Sea in the interpretation of data from the SeaWiFS satellite instrument. *Phys. Oceanogr.* **2004**, *1*, 69–79.
11. Kalinskaya, D.V.; Kabanov, D.M.; Latushkin, A.A.; Sakerin, S.M. Atmospheric aerosol optical thickness measurements in the Black sea region (2015–2016). *Atmos. Ocean. Opt.* **2017**, *6*, 489–496.
12. Kaufman, Y.J.; Tanré, D.; Boucher, O. A satellite view of aerosols in the climate system. *Nature* **2002**, *419*, 215–223. [CrossRef] [PubMed]
13. Suetin, V.S.; Korolev, S.N. Estimating Specific Features of the Optical Property Variability in the Black Sea Waters Using the Data of SeaWiFS and MODIS Satellite Instruments. *Phys. Oceanogr.* **2018**, *25*, 330–340. [CrossRef]
14. Suetin, V.S.; Korolev, S.N. Application of Satellite Data for Retrieving the Light Absorption Characteristics in the Black Sea Waters. *Phys. Oceanogr.* **2021**, *28*, 205–214. [CrossRef]
15. Korchemkina, E.N.; Shibanov, E.B.; Li, M.E. Improvement of the Atmospheric Correction Technique for Remote Investigations of Black Sea Coastal Waters. *Issled. Zemli Kosmosa* **2009**, *6*, 24–30.
16. Parshikov, S.V.; Li, M.E. Remote sensing of optically active impurities using the short-wavelength part of the spectrum. In *Automated Systems for Monitoring the State of the Marine Environment*; MGI NAS of Ukraine: Sevastopol, Ukraine, 1992; pp. 65–78.
17. Moulin, C.; Gordon, H.R.; Chomko, R.M.; Banzon, V.F.; Evans, R.H. Atmospheric correction of ocean color imagery through thick layers of Saharan dust. *Geophys. Res. Lett.* **2001**, *28*, 5–8. [CrossRef]
18. Moulin, C.; Lambert, C.E.; Dayan, U.; Masson, V.; Ramonet, M.; Bousquet, P.; Legrand, M.; Balkanski, Y.J.; Guelle, W.; Marticorena, B.; et al. Satellite climatology of African dust transport in the Mediterranean atmosphere. *J. Geophys. Res. Atmos.* **1998**, *103*, 13137–13144. [CrossRef]
19. Gordon, H.R. Evolution of Ocean Color Atmospheric Correction: 1970–2005. *Remote Sens.* **2021**, *13*, 5051. [CrossRef]
20. Wei, J.; Yu, X.; Lee, Z.; Wang, M.; Jiang, L. Improving low-quality satellite remote sensing reflectance at blue bands over coastal and inland waters. *Remote Sens. Environ.* **2020**, *250*, 112029. [CrossRef]
21. Schollaert, S.E.; Yoder, J.A.; O'Reilly, J.E.; Westphal, D.L. Influence of dust and sulfate aerosols on ocean color spectra and chlorophyll *a* concentrations derived from SeaWiFS off the U.S. east coast. *J. Geophys. Res.* **2003**, *108*, 3191. [CrossRef]
22. Mélin, F. Validation of ocean color remote sensing reflectance data: Analysis of results at European coastal sites. *Remote Sens. Environ.* **2022**, *280*, 113153. [CrossRef]
23. Kopelevich, O.V.; Saling, I.V.; Vazyulya, S.V.; Glukhovets, D.I.; Sheberstov, S.V.; Burenkov, V.I.; Karalli, P.G.; Yushmanova, A.V. *Biooptical Characteristics of the Seas Washing the Shores of the Western Half of Russia, According to Satellite Color Scanners 1998–2017*; Kopelevich, O.V., Ed.; Shirshov Institute of Oceanology: Moscow, Russia, 2018; 140p. Available online: https://optics.ocean.ru/Atlas_2019/8_Monography_2018.pdf (accessed on 14 January 2021). (In Russian)
24. Shybanov, E.B.; Papkova, A.S. Algorithm for Additional Correction of Remote Sensing Reflectance in the Presence of Absorbing Aerosol: Case Study. *Phys. Oceanogr.* **2022**, *29*, 688–706.
25. Gordon, H.R.; Wang, W. Influence of oceanic whitecaps on atmospheric correction of SeaWiFS. *Appl. Opt.* **1994**, *33*, 7754–7763. [CrossRef] [PubMed]
26. Ruddick, K.G.; Ovidio, F.; Rijkeboer, M. Atmospheric correction of SeaWiFS imagery for turbid coastal and inland waters. *Appl. Opt.* **2000**, *39*, 897–912. [CrossRef] [PubMed]
27. Feng, L.; Hou, X.; Li, J.; Zheng, Y. Exploring the potential of Rayleigh-corrected reflectance in coastal and inland water applications: A simple aerosol correction method and its merits. *ISPRS J. Photogramm. Remote Sens.* **2018**, *146*, 52–64. [CrossRef]

28. Hu, C.; Carder, K.L.; Muller-Karger, F.E. Atmospheric Correction of SeaWiFS Imagery over Turbid Coastal Waters: A Practical Method. *Remote Sens. Environ.* **2000**, *74*, 195–206. [CrossRef]
29. Hu, C.; Lee, Z.; Franz, B. Chlorophyll *a*algorithms for oligotrophic oceans: A novel approach based on three-band reflectance difference. *J. Geophys. Res. Oceans* **2012**, *117*, C01011. [CrossRef]
30. Morel, A.; Claustre, H.; Gentili, B. The most oligotrophic subtropical zones of the global ocean: Similarities and differences in terms of chlorophyll and yellow substance. *Biogeosciences* **2010**, *7*, 3139–3151. [CrossRef]
31. Shybanov, E.; Papkova, A.; Korchemkina, E.; Suslin, V. Blue Color Indices as a Reference for Remote Sensing of Black Sea Water. *Remote Sens.* **2023**, *15*, 3658. [CrossRef]
32. Shybanov, E.B.; Papkova, A.S. Features of the atmospheric correction error in the presence of an absorbing aerosol over the sea. In Proceedings of the All-Russian Conference "Modern Problems" Optics of In-Situ Waters, St. Petersburg, Russia, 25–27 October 2023; pp. 233–237.
33. Nousiainen, T.; Muinonen, K.; Räisänen, P. Scattering of light by large Saharan dust particles in a modified ray optics approximation. *J. Geophys. Res. Atmos.* **2003**, *108*, 4025. [CrossRef]
34. Redmond, H.E.; Dial, K.D.; Thompson, J.E. Light Scattering and Absorption by Wind Blown Dust: Theory, Measurment, and Recent Data. *Aeolian Res.* **2009**, *2*, 5–26. [CrossRef]
35. Min, M. Dust Opacities. *EPJ Web Conf.* **2015**, *102*, 00005. [CrossRef]
36. Shybanov, E.; Papkova, A. Differences in the Ocean Color atmospheric correction algorithms for remote sensing reflectance retrievals for different atmospheric conditions. *Sovrem. Probl. Distantsionnogo Zondirovaniya Zemli Iz Kosmosa* **2022**, *19*, 9–17. [CrossRef]
37. Papkova, A.; Kalinskaya, D.; Shybanov, E. Atmospheric correction according to the MODIS and VIIRS satellite data with considering the atmospheric pollution factor by a combination of different types of aerosol. In Proceedings of the 28th International Symposium on Atmospheric and Ocean Optics: Atmospheric Physics, Tomsk, Russia, 4–8 July 2022; Volume 12341, p. 123414G.
38. Suslin, V.V.; Sholar, S.; Martynov, O.V. Baikal regional algorithm of diffuse attenuation coefficient based on HawkEye standard level-2 products. In Proceedings of the SPIE 28th International Symposium on Atmospheric and Ocean Optics: Atmospheric Physics, Tomsk, Russia, 4–8 July 2022; Volume 12341, p. 1234148. [CrossRef]
39. Gregg, W.W.; Conkright, M.E. Decadal changes in global ocean chlorophyll. *Geophys. Res. Lett.* **2002**, *29*, 20-1–20-4. [CrossRef]
40. Available online: https://oceancolor.gsfc.nasa.gov/data/hawkeye/on-orbit-changes/ (accessed on 17 January 2022).
41. *NASA/TM 2002–211617*; The SeaWiFS Bio-Optical Archive and Storage System (SeaBASS): Current Architecture and Implementation. Goddard Space Flight Center: Greenbelt, MD, USA, 2002.
42. Stumpf, R.P.; Arnone, R.A.; Gould, R.W., Jr.; Martinolich, P.M.; Ransibrahmanakul, V. A Partially coupled ocean-atmosphere model for retrieval of water-leaving radiance from SeaWiFS in coastal waters. In *Algorithm Updates for the Fourth SeaWiFS Data Reprocessing*; SeaWiFS Postlaunch Technical Report Series; NASA, Goddard Space Flight Center: Greenbelt, MD, USA, 2003; Volume 22.
43. Carder, K.L.; Chen, F.R.; Lee, Z.P.; Hawes, S.K.; Kamykowski, D. Semianalytic Moderate-Resolution Imaging Spec-trometer algorithms for chlorophyll a and absorption with bio-optical domains based on nitrate-depletion temperatures. *J. Geophys. Res. Ocean.* **1999**, *104*, 5403–5422. [CrossRef]
44. Gould, R.W., Jr.; Arnone, R.A.; Martinolich, P.M. Spectral dependence of the scattering coefficient in case 1 and case 2 waters. *Appl. Opt.* **1999**, *38*, 2377–2383. [CrossRef] [PubMed]
45. Gordon, H.R.; Brown, O.B.; Evans, R.H.; Brown, J.W.; Smith, R.C.; Baker, K.S.; Clark, D.K. A semianalytic radiance model of ocean color. *J. Geophys. Res. Atmos.* **1988**, *93*, 10909–10924. [CrossRef]
46. Bricaud, A.; Morel, A.; Babin, M.; Allali, K.; Claustre, H. Variations of light absorption by suspended particles with chlorophyll *a* concentration in oceanic (case 1) waters: Analysis and implications for bio-optical models. *J. Geophys. Res. Oceans* **1998**, *103*, 31033–31044. [CrossRef]
47. Available online: https://oceancolor.gsfc.nasa.gov/data/hawkeye/data-collection-and-processing/ (accessed on 19 January 2022).
48. Zibordi, G.; Holben, B.; Slutsker, I.; Giles, D.; D'alimonte, D.; Mélin, F.; Berthon, J.-F.; Vandemark, D.; Feng, H.; Schuster, G.; et al. AERONET-OC: A Network for the Validation of Ocean Color Primary Products. *J. Atmos. Ocean. Technol.* **2009**, *26*, 1634–1651. [CrossRef]
49. Zibordi, G.; Mélin, F.; Berthon, J.-F.; Talone, M. In situ autonomous optical radiometry measurements for satellite ocean color validation in the Western Black Sea. *Ocean Sci.* **2015**, *11*, 275–286. [CrossRef]
50. Thuillier, G.; Hersé, M.; Labs, D.; Foujols, T.; Peetermans, W.; Gillotay, D.; Simon, P.C.; Mandel, H. The Solar Spectral Irradiance from 200 to 2400 nm as Measured by the SOLSPEC Spectrometer from the Atlas and Eureca Missions. *Sol. Phys.* **2003**, *214*, 1–22. [CrossRef]
51. Sakerin, S.M.; Kabanov, D.M.; Rostov, A.P.; Turchinovich, S.A.; Knyazev, V.V. Sun photometers for measuring spectral air transparency in stationary and mobile conditions. *Atmos. Ocean. Opt.* **2013**, *26*, 352–356. [CrossRef]
52. Varenik, A.V.; Kalinskaya, D.V.; Myslina, M.A. Investigation of airborne particulate matter in the atmosphere of the Black sea coastal zone based on the measured and satellite data. *Phys. Oceanogr.* **2021**, *28*, 326–337. [CrossRef]
53. Available online: https://ntm.ru/products/150/8342 (accessed on 30 January 2021).
54. Stein, A.F.; Draxler, R.R.; Rolph, G.D.; Stunder, B.J.B.; Cohen, M.D.; Ngan, F. NOAA's HYSPLIT Atmospheric Transport and Dispersion Modeling System. *Bull. Am. Meteorol. Soc.* **2015**, *96*, 2059–2077. [CrossRef]

55. Omar, A.H.; Winker, D.M.; Vaughan, M.A.; Hu, Y.; Trepte, C.R.; Ferrare, R.A.; Lee, K.-P.; Hostetler, C.A.; Kittaka, C.; Rogers, R.R.; et al. The CALIPSO Automated Aerosol Classification and Lidar Ratio Selection Algorithm. *J. Atmos. Ocean. Technol.* **2009**, *26*, 1994–2014. [CrossRef]
56. Omar, A.H.; Tackett, J.; Al-Dousari, A. CALIPSO Observations of Sand and Dust Storms and Comparisons of Source Types near Kuwait City. *Atmosphere* **2022**, *13*, 1946. [CrossRef]
57. Sofiev, M.; Siljamo, P.; Ranta, H.; Linkosalo, T.; Jaeger, S.; Rasmussen, A.; Rantio-Lehtimaki, A.; Severova, E.; Kukkonen, J. A numerical model of birch pollen emission and dispersion in the atmosphere. Description of the emission module. *Int. J. Biometeorol.* **2013**, *57*, 45–58. [CrossRef]
58. Available online: https://silam.fmi.fi/dust.html (accessed on 1 April 2023).
59. Gobron, N.; Morgan, O.; Adams, J.; Brown, L.A.; Cappucci, F.; Dash, J.; Lanconelli, C.; Marioni, M.; Robustelli, M. Evaluation of Sentinel-3A and Sentinel-3B ocean land colour instrument green instantaneous fraction of absorbed photosynthetically active radiation. *Remote Sens. Environ.* **2021**, *270*, 112850. [CrossRef]
60. Bailey, S.W.; Werdell, P.J. A multi-sensor approach for the on-orbit validation of ocean color satellite data products. *Remote Sens. Environ.* **2006**, *102*, 12–23. [CrossRef]
61. Wang, M.; Son, S.; Harding, L.W., Jr. Retrieval of diffuse attenuation coefficient in the Chesapeake Bay and turbid ocean regions for satellite ocean color applications. *J. Geophys. Res. Oceans* **2009**, *114*, C11001. [CrossRef]
62. Available online: https://aeronet.gsfc.nasa.gov/new_web/Documents/Inversion_products_V2.pdf (accessed on 21 April 2021).
63. Available online: https://www-calipso.larc.nasa.gov/products/lidar/browse_images/production/ (accessed on 9 May 2023).
64. Kim, M.-H.; Omar, A.H.; Tackett, J.L.; Vaughan, M.A.; Winker, D.M.; Trepte, C.R.; Hu, Y.; Liu, Z.; Poole, L.R.; Pitts, M.C.; et al. The CALIPSO version 4 automated aerosol classification and lidar ratio selection algorithm. *Atmos. Meas. Tech.* **2018**, *11*, 6107–6135. [CrossRef] [PubMed]
65. Kalinskaya, D.V.; Suslin, V.V. A simple method for identifying surface aerosol sources based on back-path analysis results. *Fundam. Appl. Hydrophys.* **2015**, *8*, 59–67.
66. Suetin, V.S.; Kucheryavy, A.A.; Suslin, V.V.; Korolev, S.N. Concentration of phytoplankton pigments in the northwestern part of the Black Sea based on data of measurements by satellite color scanner CZCS. *Mar. Hydrophys. J.* **2000**, *2*, 74–82.
67. Khalturin, V.I.; Suetin, V.S.; Shutikov, S.P. *On a Low-Parameter Model of the Optical Properties of Sea Water*; Dep. VINITI (Moscow): Moscow, Russia, 1984; No. 3548-84; 13p.
68. D'alimonte, D.; Shybanov, E.B.; Zibordi, G.; Kajiyama, T. Regression of in-water radiometric profile data. *Opt. Express* **2013**, *21*, 27707–27733. [CrossRef] [PubMed]
69. Seegers, B.N.; Stumpf, R.P.; Schaeffer, B.A.; Loftin, K.A.; Werdell, P.J. Performance metrics for the assessment of satellite data products: An ocean color case study. *Opt. Express* **2018**, *26*, 7404–7422. [CrossRef]
70. Zibordi, G.; Kwiatkowska, E.; Mélin, F.; Talone, M.; Cazzaniga, I.; Dessailly, D.; Gossn, J.I. Assessment of OLCI-A and OLCI-B radiometric data products across European seas. *Remote Sens. Environ.* **2022**, *272*, 112911. [CrossRef]